Poleward moving auroral arcs observed at the South Pole Station and the interpretation by field line resonances

Y.-M. Tanaka,[1] Y. Ebihara,[2] S. Saita,[3] A. Yoshikawa,[4] Y. Obana,[5] and A. T. Weatherwax[6]

[1]   We investigate the characteristics of poleward moving auroral arcs (PMAAs) observed with the all-sky monochromatic imager at the South Pole Station (74.3°CGLAT) in the interval 08:00–11:00 MLT on July 8, 2004. During this period, Pc 5 geomagnetic pulsations are also observed as well as quasi-stationary auroral patches (QSAPs), which keep their forms, luminosities, and locations for up to several hours. It is demonstrated that the PMAAs, Pc 5 pulsations in the north-south component, and oscillations in the drift of the QSAPs in the east-west direction have similar dominant periods and are well correlated with each other. The oscillatory ionospheric plasma drifts accompanying the PMAAs are extracted from the horizontal motion of the QSAPs and are found to propagate poleward with the PMAAs. The phase relations of the PMAAs and Pc 5 pulsations in the northward component with respect to the westward drift velocity of the QSAPs are close to anti-phase and in-phase, respectively. To examine whether these phenomena can be interpreted by field line resonances (FLRs), we perform a numerical simulation using a horizontally two-dimensional model that consists of the auroral acceleration region and the ionosphere with time-evolution conductivity. The results indicate that the observed data can be well explained by the FLR model with realistic physical parameters, except for the phase relation of the PMAAs with respect to the Pc 5 pulsations and the QSAPs.

1. Introduction

[2] Poleward moving auroral forms (PMAFs) observed in the high-latitude ionosphere at around 75° magnetic latitude (MLAT) on the dayside around 9–15 magnetic local time (MLT) are a manifestation of the interaction between the solar wind and the magnetosphere. PMAFs are characterized by a lifetime of 2–10 min, a recurrence period of 3–15 min, and a velocity of the poleward motion of less than 1.5 km/sec [cf. *Sandholt et al.*, 1990]. They are generally related to dayside reconnection and flux transfer events (FTEs). The occurrence frequency of PMAFs strongly depends on the solar

wind parameters, in particular, B_z and B_y of the interplanetary magnetic field (IMF); PMAFs occur most frequently for IMF $B_z < 0$ conditions but can also occur for $B_z > 0$ conditions [*Fasel*, 1995; *Drury et al.*, 2003]. A positive or negative B_y enhances the observation of PMAFs in the prenoon or postnoon sectors in the Northern Hemisphere, respectively, and the B_y dependence of PMAFs is antisymmetric in the Southern Hemisphere [*Karlson et al.*, 1996; *Sandholt et al.*, 1993; *Drury et al.*, 2003].

[3] Quasiperiodic PMAFs correlated with ULF pulsations are occasionally related to field line resonances (FLRs) [*Tamao*, 1964; *Southwood*, 1974; *Chen and Hasegawa*, 1974; *Milan et al.*, 1999a, 1999b, 2001; *Kozlovsky and Kangas*, 2002]. *Milan et al.* [1999a, 2001] examined PMAFs co-located with the convection reversal boundary in the postnoon sector and showed that the meridian scan data of PMAFs have the characteristics of FLRs, such as wave-like oscillations with a similar dominant frequency to the geomagnetic pulsations, occasional harmonic oscillations, and a 180° phase change across the latitude of maximum emission intensity. *Kozlovsky and Kangas* [2002] investigated PMAFs observed equatorward of the convection reversal (i.e., on closed field lines) at 10:00–13:00 MLT using data from the all-sky camera and European Incoherent Scatter (EISCAT) VHF radar. They found that the spectra of the eastward plasma flow measured by the radar show clear peaks corresponding to the eigenfrequency of the FLR oscillations and suggested

[1]National Institute of Polar Research, Tokyo, Japan.
[2]Research Institute for Sustainable Humanosphere, Kyoto University, Kyoto, Japan.
[3]Transdisciplinary Research Integration Center, Research Organization of Information and Systems, Tokyo, Japan.
[4]Department of Earth and Planetary Sciences, Kyushu University, Fukuoka, Japan.
[5]Department of Engineering Science, Osaka Electro-Communication University, Osaka, Japan.
[6]Department of Physics, Siena College, Latham, New York, USA.

Corresponding author: Y.-M. Tanaka, National Institute of Polar Research, 10-3 Midori-cho, Tachikawa, Tokyo 190-8518, Japan. (ytanaka@nipr.ac.jp)

that the PMAFs are a result of interference between the eigenmode toroidal oscillations on different L shells. In order to distinguish this type of event from the former-stated PMAFs, we refer to them as poleward moving auroral arcs (PMAAs), according to *Kozlovsky and Kangas* [2002]. In this paper, we define PMAAs as occurring in the closed field lines and associated with FLRs, whereas PMAFs occur on or in the vicinity of the open–close boundary mainly due to dayside reconnection.

[4] Even in the region far from the dayside cusp, PMAAs have been detected, for example, in the auroral zone in the nighttime [*Samson et al.*, 1991, 1996]. *Samson et al.* [1996] demonstrated that meridian scans of all-sky images obtained in the nighttime auroral region show poleward moving discrete arcs and very clear ULF oscillations with the dominant frequency expected from the FLRs. Furthermore, other than the optical aurora, Pc 5 pulsations observed over a wide range of MLT by the STARE radar have often shown poleward moving structures in the backscatter echo and the FLR-related spatial structures in the amplitude and phase of the east-west (E-W) plasma velocity [*Walker et al.*, 1979; *Walker and Greenwald*, 1981; *Poulter*, 1982].

[5] Another aurora phenomenon closely related to ULF geomagnetic pulsations is oscillations in the drift of auroral patches or diffuse aurora [*Oguti et al.*, 1987; *Yamamoto et al.*, 1988]. The motion of auroral patches observed with all-sky TV imagers provides information on the two-dimensional (2-D) distribution of the plasma convection. *Oguti et al.* [1987] examined spatial distribution of drifts of non-pulsating auroral patches in the evening sector and found that the auroral patches oscillate primarily in the E-W direction associated with concurrent magnetic pulsations and the oscillations of the patches are consistent with the electrostatic electric field accompanied by the pulsations.

[6] Recently, *Ebihara et al.* [2007] reported quasi-stationary auroral patches (QSAPs) observed at the South Pole Station ($-74.3°$CGLAT) on the dayside at 09:00–14:00 MLT, which keep their form, location, and luminosity for up to several hours. They suggested that the QSAPs were generated in the central plasma sheet where the field lines are closed, because the QSAPs were observed at 557.7 nm equatorward of a longitudinally elongated arc detected at 630.0 nm at 78–79°CGLAT, which is probably associated with the low-latitude boundary layer (LLBL) or the cleft region. Furthermore, the QSAPs showed periodic fluctuations of their drift velocity in the E-W direction and the fluctuations were well correlated with Pc 5 pulsations observed in the north-south (N-S) component. The relationship between the drift velocity of QSAPs, corresponding to the ionospheric electric field, and Pc 5 pulsations observed on the ground can be explained by the ionospheric current controlled by Ohm's law.

[7] This paper follows up the research of *Ebihara et al.* [2007]. We newly analyze PMAAs (that were not reported by *Ebihara et al.* [2007]) detected simultaneously with the QSAPs and Pc 5 pulsations in the same period analyzed by *Ebihara et al.* [2007]. The advantage of this study is that the QSAPs appeared simultaneously with the PMAAs for several hours and thus the spatial distribution of the ionospheric drift velocity associated with the PMAAs can be deduced from the horizontal motion of the QSAPs. In addition, we carry out a numerical simulation to examine whether these three

phenomena, PMAAs, QSAPs, and Pc 5 pulsations, can be interpreted by the FLR mechanism.

2. Data Set and Conditions During the Events

[8] The data used in this paper are almost the same as those used by *Ebihara et al.* [2007]. We analyzed data recorded with the all-sky imager (ASI) and the fluxgate magnetometer at the South Pole Station (SPA) during the interval 11:00–17:00 UT, corresponding to ~07:30–13:30 MLT (MLT ~ UT − 3.5 h at SPA), on July 8, 2004. In addition to these data, we analyzed magnetic data from Iqaluit (IQA), which is a station located close to the geomagnetic conjugate of SPA in the Northern Hemisphere. The ASI consists of a 180° field-of-view lens (f = 6 mm, F = 1.4), a back-illuminated air-cooled CCD camera with a resolution of 512 × 512 pixels, and an automated filter changer with 557.7-nm and 630.0-nm monochromatic filters. The images at 557.7 nm were recorded with an exposure time of 8 s every 32 s during the period we analyzed. The absolute luminosities were calibrated using the integrating sphere at the National Institute of Polar Research, Japan.

[9] According to *Ebihara et al.* [2007], the solar wind and geomagnetic conditions were very quiet during this interval. The solar wind speed detected by the ACE satellite was about 310–340 km/s. The IMF B_z was stably positive except for short periods around 14:20 and 15:00–15:30 UT. K_P and AE indices were 0+ to 1− and below 110, respectively.

3. Observational Results

[10] Figure 1 shows the 557.7-nm images taken at SPA in the interval 12:14:56–12:25:42 UT as examples of PMAAs and QSAPs. The images were mapped to 110 km altitude. In this figure the PMAAs passed across the zenith at about 12:17:05, 12:21:23, and 12:25:42 UT from magnetic north to south (i.e., from low latitude to high latitude). Stable auroral patches can be seen on the magnetic north side of the images. The arrows in the images indicate the drift velocity of the auroral patches calculated from two consecutive images by minimum mean square error (MMSE) analysis [*Ebihara et al.*, 2007]. In this paper we identified the auroral patches by a visual scan and manually determined the position of the scanning area for the MMSE analysis, which is different from the method used by *Ebihara et al.* [2007], who fixed the scanning area. We set the scanning area and the kernel area for the MMSE to 75 km × 75 km and 37.5 km × 37.5 km, respectively [see *Ebihara et al.*, 2007]. It appears that the QSAPs oscillate primarily in the magnetic E-W direction in correlation with the passage of the PMAAs.

[11] Figure 2 shows the keogram of 557.7 nm intensity in the magnetic N-S direction and the magnetic field observed with the fluxgate magnetometer at SPA in the interval 11:00–17:00 UT. The keogram was made from images mapped to 110 km altitude and its vertical axis represents the distance from the zenith. The quasiperiodic intensifications seen in the keogram correspond to the PMAAs. The intensifications due to the PMAAs can be clearly seen in the interval 11:30–14:00 UT, where Pc 5 pulsations occurred predominantly in the H and Z components. The bright auroral patches reached the zenith around 14:00 UT and moved southward and also westward (not shown here). After
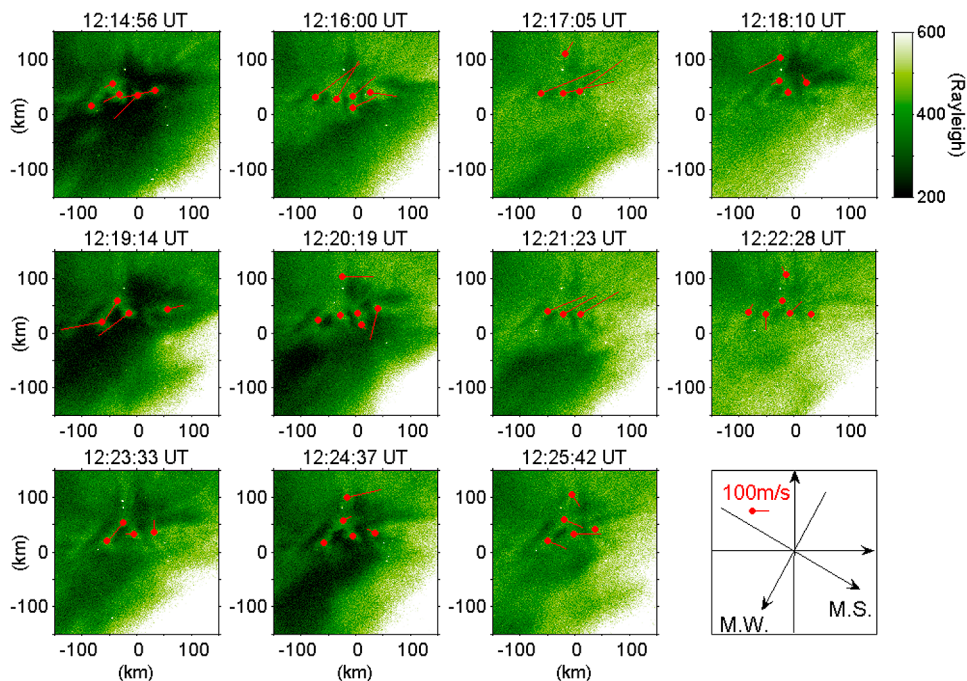
Figure 1. Auroral images at 557.7 nm taken at SPA in the interval 12:14:56–12:25:42 UT. The images were mapped to 110 km altitude and the top and right of the images correspond to the geographic north and east, respectively. The arrows in the images show the drift velocity of the selected auroral patches calculated from two consecutive images by MMSE analysis.

15:30 UT, the PMAAs could not be identified and the periods of the Pc 5 pulsations were longer than before 15:00 UT.

[12] It should be noted that in this paper the magnetic north is defined so as to be perpendicular to the PMAAs, that is, 25° W in geographic coordinates. The angle is similar to the declination at SPA, −29°, calculated by the IGRF (International Geomagnetic Reference Field) model. The magnetic N-S direction (25° W in geographic coordinates) is a rough estimation, because the PMAAs detected in this study were broad bands, as seen in Figure 1.

[13] We here explain the coordinate system used in this study. The origin is placed at SPA and the x axis and y axis are directed geomagnetically westward and southward, respectively. This coordinate system is also adopted for the numerical simulation in section 5.

[14] Figure 3 shows an expanded view of Figure 2 in the interval 11:50–12:30 UT. The keogram in the magnetic E-W direction was added to Figure 3b. In order to highlight the PMAAs, the running average of the keogram over about 672 s (21 data points) was subtracted from the keogram in Figure 2. It can be confirmed that the auroral arcs
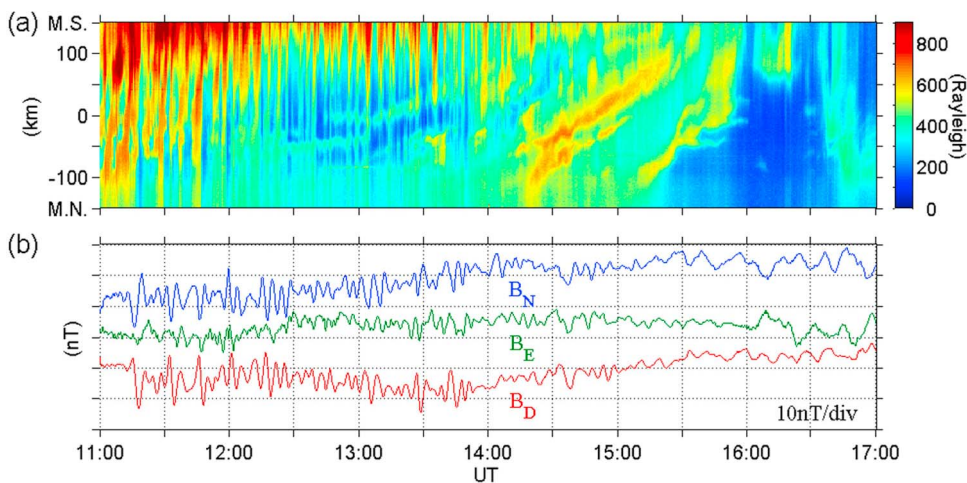

Figure 2. (a) Keogram along the magnetic meridian derived from auroral 557.7-nm images in the interval 11:00–17:00 UT. (b) Magnetic field measured with the fluxgate magnetometer at SPA.
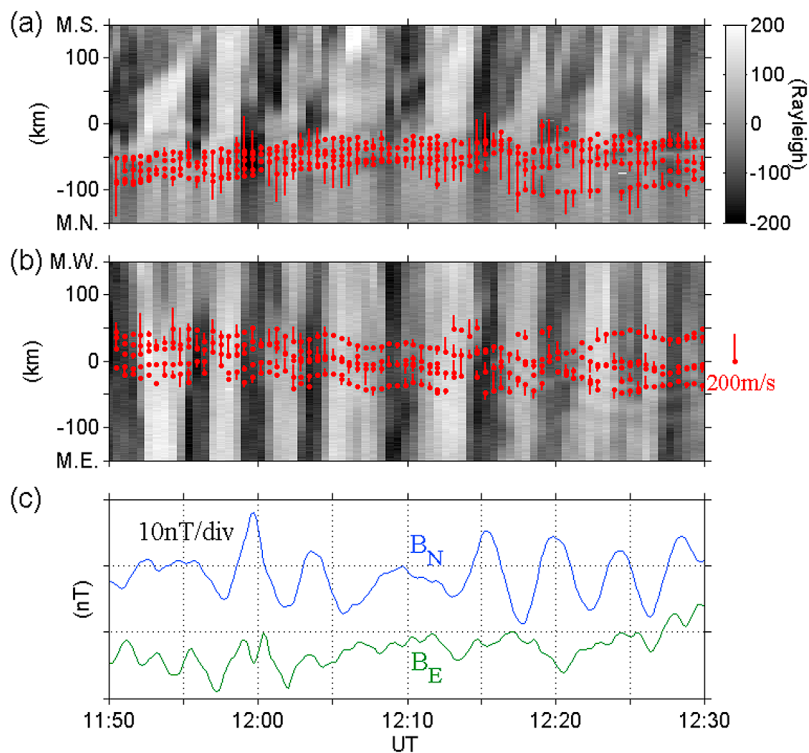
Figure 3. (a) N-S keogram of the 557.7-nm emission in the interval 11:50–12:30 UT. The running mean has been subtracted from the keogram. Note that the length of the arrows in the panel shows the E-W drift velocity of QSAPs. The solid circles exhibit the y coordinates of the QSAPs location. (b) E-W keogram of the 557.7-nm emission with the arrows indicating the N-S drift velocity of the QSAPs. The solid circles show the x coordinates of the QSAPs location. (c) Magnetic field in the N-S and E-W components.

propagated southward (poleward). The propagation velocities of the PMAAs observed in this interval are between 1 and 3 km/sec. The solid circles in the keograms exhibit the y coordinates of the locations of the selected QSAPs events for the N-S keogram (Figure 3a) and the x coordinates for the E-W keogram (Figure 3b). The vertical arrows show the drift velocity of the QSAPs, which indicate the E-W component for the N-S keogram and the N-S component for the E-W keogram. The upward arrows correspond to the westward drift in Figure 3a and the southward drift in Figure 3b. It is clearly evident that there is a one-to-one correspondence between the PMAAs, the Pc 5 pulsations in the N-S component (B_N), and the oscillations in the E-W drift velocity of the QSAPs. It appears that these three phenomena are oscillating with similar periods and specific phase relations. On the other hand, there are no apparent relationships of the N-S drift velocity of the QSAPs (Figure 3b) and the magnetic field in the E-W component (B_E in Figure 3c) to the PMAAs.

[15] In order to investigate the latitudinal phase structure of the oscillations in the drift of the QSAPs, the averaged westward drift velocities of the QSAPs located at low latitudes (-120 km $\leq$ y < -30 km), around the zenith (-30 km $\leq$ y < 30 km), and at high latitude (30 km $\leq$ y < 120 km) are separately presented in Figure 4. The QSAPs located within -50 km $\leq$ x ≤ 50 km were used for averaging. The lack of data in some intervals means that no QSAPs were identified in the intervals within the specified y-range. This figure

indicates that the oscillations in the E-W drift of the QSAPs at high latitudes tend to lag behind those at low latitudes, in particular, in the interval 12:30–14:30 UT. The phase difference is ambiguous after 15:00 UT, because the number of the identified QSAPs was small.

[16] Figure 5 illustrates a relationship between the intensity of PMAAs (I_{5577}), the magnetic field in the N-S component, and the E-W drift velocity of the QSAPs in the interval 12:50–13:20 UT. I_{5577} shows the intensity of the keogram averaged over y from -30 km to 30 km. V_W is the averaged westward drift velocity of the QSAPs located at -30 km $\leq$ y < 30 km. This figure indicates that the phase relation between V_W and B_N is close to in-phase and I_{5577} is nearly anti-phase with respect to V_W and B_N. The dominant periods calculated by the spectral analysis are very similar to each other, i.e., 302, 299, and 299 s for B_N, V_W, and I_{5577}, respectively. The correlation coefficient and the phase difference are -0.74 and $-8°$ between I_{5577} and V_W and 0.93 and $-31°$ between B_N and V_W, where the negative value of the phase difference means that I_{5577} and B_N lag behind V_W. A similar phase relationship was obtained at 12:00–12:30 UT, shown in Figure 3. Since there were few QSAPs located around the zenith (-30 km $\leq$ y < 30 km) in this interval, V_W was calculated for -120 km $\leq$ y < -30 km. For the interval 12:00–12:30 UT, the dominant periods are 302, 293, and 293 s for B_N, V_W, and I_{5577}, and the correlation coefficient and the phase difference are -0.76 and $-27°$ between I_{5577} and V_W and 0.90 and $-40°$ between B_N and V_W. If we use
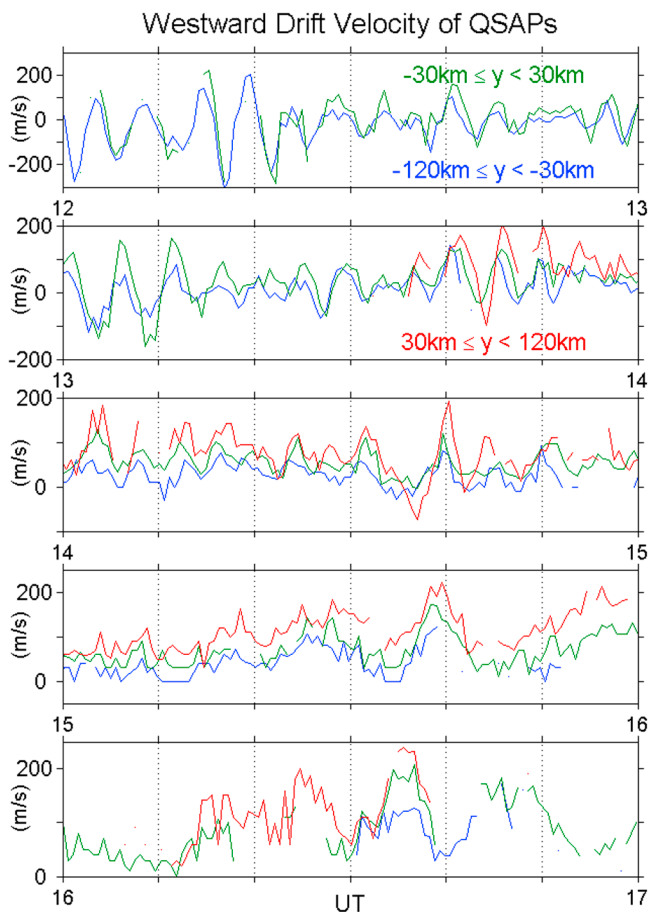
Figure 4. Latitudinal dependence of the westward drift velocity of the QSAPs. The blue, green, and red lines show the averaged velocities of the QSAPs in the areas -120 km $\leq y < -30$ km, -30 km $\leq y < 30$ km, and 30 km $\leq y < 120$ km, respectively. The QSAPs located within -50 km $\leq x \leq 50$ km were used for averaging.

V_W around the zenith as the reference for the phase difference, the phase difference is closer to $0°$ because V_W around the zenith tends to lag behind that at low latitude, as shown in Figure 4.

[17] Figure 6 shows the magnetic field observed in the interval 11:00–14:00 UT at Iqaluit (IQA), which is close to the geomagnetic conjugate point of SPA in the Northern Hemisphere, and at SPA. It was confirmed that Pc 5 pulsations were also observed at IQA and their waveform is quite similar to that at SPA. While the amplitude in B_N and B_D (downward) was greater at SPA than at IQA, B_E was slightly greater at IQA than at SPA. The good correlation of the Pc 5 pulsations between SPA and IQA supports the standing field-line oscillations.

4. Summary of Observational Results

[18] The observational results are summarized as follows;
[19] 1. PMAAs, QSAPs, and Pc 5 pulsations were simultaneously observed at SPA at 11:30–14:30 UT (08:00–11:00 MLT) on July 8, 2004. The quasiperiodic PMAAs, the oscillations in the E-W drift velocity of the QSAPs, and
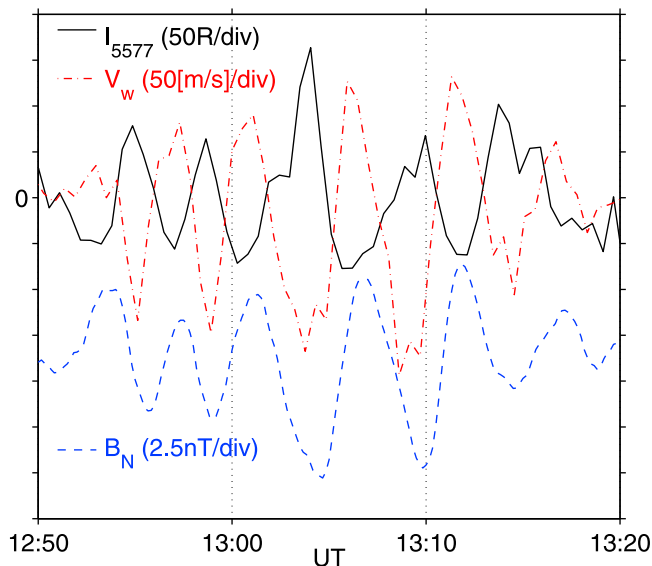

Figure 5. Relationship among the 557.7-nm intensity (I_{5577}) derived from the N-S keogram, drift velocity in the E-W direction of the QSAPs (V_w), and magnetic variation in the N-S component (B_N) in the interval 12:50–13:20 UT. I_{5577} and V_w were averaged in the region -30 km $\leq y < 30$ km, i.e., around zenith. The intensification of I_{5577} corresponds to the passage of the PMAAs through the zenith.

the Pc 5 pulsations in the N-S component correlated well with each other and had similar periods.
[20] 2. PMAAs were clear and the period of the Pc 5 pulsations is shorter before 14:30 UT (11:00 MLT), whereas the PMAAs were not identified and the Pc 5 pulsations have a longer period after 15:30 UT (12:00 MLT).
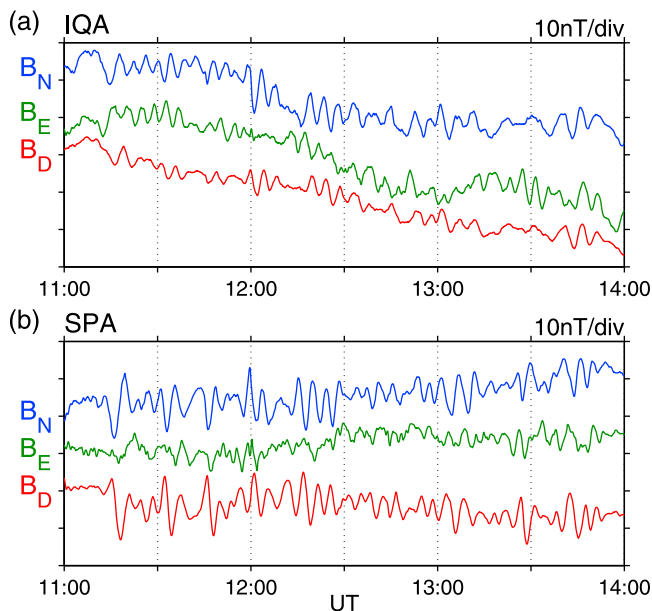[21] 3. The oscillations in the westward velocity of the QSAPs (V_W) at high latitudes lag behind those at low

Figure 6. Magnetic variations observed in the interval 11:00–14:00 at (a) IQA and (b) SPA.

latitudes. This lag indicates a poleward propagation of the oscillations of the QSAPs.

[22] 4. V_W around the zenith was close to in-phase with respect to the northward magnetic variation (B_N) and anti-phase with respect to the luminosity variation due to the PMAAs around the zenith (I_{5577}). The phase differences are about $-10°$ between I_{5577} and V_W and about $-30°$ between B_N and V_W.

[23] 5. Coherent Pc 5 pulsations were also observed at IQA, which is located close to the magnetic conjugate of SPA in the Northern Hemisphere.

[24] In item 1, the good correlation between the PMAAs (or PMAFs) and Pc 5 pulsations has already been reported in many papers. Furthermore, the relationship between the oscillations in the drift of the auroral patches or diffuse aurora and Pc 5 pulsations has also been analyzed in detail [Oguti et al., 1987; Yamamoto et al., 1988; Ebihara et al., 2007]. This analysis showed that the auroral patches oscillate primarily in the E-W direction and the oscillations in the drift are consistent with the ionospheric electric field associated with ULF pulsations observed in the N-S component on the ground, which is consistent with our results. Oguti et al. [1987] further clarified that the oscillations in the E-W drift of non-pulsating auroral patches in the evening sector propagate poleward, associated with Pc 5 pulsations. Item 3 agrees with this previous result.

[25] The events analyzed by Yamamoto et al. [1988] are similar to those in this paper, although they were of a diffuse aurora, including a pulsating aurora, observed in the auroral zone in the dawn sector (around 04:30–07:30 MLT). They showed that the activation region of aurora quasiperiodically propagates toward the northwest, corresponding to the PMAAs, synchronized with Pc 5 pulsations. They also found that oscillations in the eastward drift of the auroral patches are synchronized with Pc 5 pulsations. Our observations have for the first time shown the relationship between these three phenomena (PMAAs, Pc 5 pulsations, and auroral patches) at very high latitude (74.3 CGLAT) in the interval 08:00–11:00 MLT.

[26] As Ebihara et al. [2007] have already shown, the field lines where the QSAPs were observed were closed and connected to the central plasma sheet, because the QSAPs were observed at 557.7 nm equatorward of a longitudinally elongated arc detected at 630.0 nm, which is related to the LLBL or the cleft region. The coherent Pc 5 pulsations observed both at SPA and IQA (item 5) support the magnetic field lines from the SPA and IQA being closed and forming standing waves. In addition to these facts, the solar wind speed was slow and the IMF B_z was northward during this period. Farrugia et al. [2000] have reported that in such northward IMF conditions, ULF pulsations associated with the FLRs were observed simultaneously with oscillations in aurora luminosity at 0900–1000 MLT and 70–80° magnetic latitudes. Therefore, it is concluded that the FLR model is more suitable for the generation of the PMAAs shown in this paper than the dayside reconnection model.

5. Numerical Simulation and Discussion

[27] In this section, we perform a numerical simulation to examine whether the observed results can be explained by the FLR model with realistic values of the physical parameters.

The simulation is based on the magnetosphere–ionosphere coupling model introduced by Janhunen and Huuskonen [1993], which includes the auroral acceleration region (AAR) and variable ionospheric conductivity. Our model, however, does not include the magnetosphere and consists of only the AAR and the ionosphere. The model is horizontally two-dimensional (2-D) except for the electron density distribution in the ionosphere, which is calculated in three dimensions. We adopted a Cartesian coordinate system with the origin at SPA, the y axis geomagnetically southward (i.e., poleward), the x axis westward, and the z axis vertically upward. The ambient magnetic field lines are assumed to be parallel to the z axis.

[28] We assumed that the Knight relation is satisfied for the field-aligned current (FAC) in the AAR [Knight, 1973] and the ionospheric current is controlled by Ohm's law under the thin-shell assumption of the ionosphere. We solve the current continuity equations on the boundary between the magnetosphere and the AAR, and the boundary between the AAR and the ionosphere:

$$j_{z,M} = K\Delta_\| \Phi \qquad (1)$$

$$= \Sigma_P \nabla_\perp^2 \Phi_I + \nabla_\perp \Sigma_P \cdot \nabla_\perp \Phi_I - \hat{\mathbf{e}}_z \cdot (\nabla_\perp \Sigma_H \times \nabla_\perp \Phi_I), \qquad (2)$$

where $j_{z,M}$ is the FAC in the magnetosphere, K and $\Delta_\| \Phi$ are the Lyons–Evans–Lundin constant and the parallel potential drop in the AAR, respectively [Lyons et al., 1979; Fridman and Lemaire, 1980]. The right-hand side of (2) comes from the convergence of the ionospheric current, and Σ_P, Σ_H, and Φ_I are the height-integrated Pedersen and Hall conductivities and the electric potentials on the ionosphere, respectively. If $j_{z,M}$, K, Σ_P, and Σ_H are given, we can solve (1) for $\Delta_\| \Phi$ and (2) for $\Phi_I \cdot j_{z,M}$ is given as the source associated with the FLRs, as described later. We solved (2) for Φ_I by the finite difference method. We adopted the alternating direction implicit (ADI) algorithm with the boundary conditions of Dirichlet ($\Phi_I = 0$) in the y direction and Nuemann in the x direction.

[29] Σ_P and Σ_H are time-dependent and were obtained from

$$\Sigma_{P,H} = \int F_{P,H}(z) n(x,y,z,t) dz, \qquad (3)$$

where $n(x, y, z, t)$ is the electron number density and $F_{P,H}(z)$ is the conductivity per unit electron density. $F_{P,H}(z)$ is a function of only z and is obtained from the number densities of the neutral gas (n_{N_2}, n_{O_2}, n_O) and ions (n_{O^+}, $n_{O_2^+}$, n_{NO^+}), the temperature of the ion, electrons, and neutrals (T_i, T_e, T_n), and the ambient magnetic field strength (B_0). These parameters were derived from the MSISE90, IRI 2001, and IGRF models [Hedin, 1991; Bilitza, 2001; International Association of Geomagnetism and Aeronomy, Division V, Working Group VMOD: Geomagnetic Field Modeling, 2005].

[30] The distribution of n is calculated from the evolution equation of n shown by

$$\frac{\partial n}{\partial t} + \nabla_\perp \cdot (n\mathbf{v}_\perp) = q_0 + q_{QSAPs} + q_P - \alpha n^2 \qquad (4)$$

where $\mathbf{v}_\perp$, q_0, q_{QSAPs}, q_P, and α are the ionospheric plasma velocity, the background ion production rate, the ion production rate associated with the QSAPs, the ion production rate due to the electron precipitation, and the effective recombination coefficient. Since $\mathbf{v}_\perp$ is the E × B drift, it is calculated from Φ_I and B_0. Equation (4) was solved for n by the forward Euler method.

[31] q_P was calculated according to *Rees* [1989], i.e.,

$$q_P = \pi \int \left[\frac{\rho(z)\lambda(z,E)E}{\Delta\varepsilon_{ion}R(E)} f\left(E, \Delta_{//}\Phi\right) \right] dE, \qquad (5)$$

where $\rho(z)$ is the atmospheric mass density, $\lambda(z, E)$ is the energy dissipation function, E is the energy, $\Delta\varepsilon_{ion}$ is the energy for producing a pair of ion, $R(E)$ is the range of the incident electrons with energy E, and $f(E, \Delta_{\|}\Phi)$ is the differential directional number flux of precipitating electrons. We assumed the isotropic pitch angle distribution for the incident electrons. Detailed values of these parameters are given in the appendix of *Tanaka et al.* [2011].

[32] In the AAR, f was assumed to be the accelerated Maxwellian distribution given by

$$f = \frac{n_M}{\sqrt{2\pi^3 m_e k_B^3 T_M^3}} E \exp\left(-\frac{E - e\Delta_{\|}\Phi}{k_B T_M}\right) \left(E \geq e\Delta_{\|}\Phi\right), \qquad (6)$$

where k_B, m_e, e, n_M, and T_M are the Boltzman constant, the electron mass, the electric charge, the source plasma density, and the magnetospheric electron temperature. n_M and T_M were assumed to be constant in this paper, so q_P are dependent on $\Delta_{\|}\Phi$ only.

[33] According to *Janhunen and Huuskonen* [1993], q_0 is expressed by

$$q_0 = \alpha \left\{ \Sigma_{H,0} n_0 \exp\left[-\left(\frac{z - z_p}{w}\right)^2 \right] \right\}^2, \qquad (7)$$

where we assumed the height profile of the electron density for the quiet condition, determined by $\Sigma_{H,0}$, n_0, z_p, and w. We set z_p to 124 km and w to 15 km. n_0 was set so that $q_0(z)$ produces a uniform background Hall conductivity of $\Sigma_H = \Sigma_{H,0}$ in the case when q_P and q_{QSAPs} vanish. Since the electron density profile is fixed when $\Sigma_{H,0}$ is set, the background Pederson conductivity is also obtained and is close to $\Sigma_{H,0}$.

[34] q_{QSAPs} was also calculated in a similar way to q_0, but $\Sigma_{H,QSAPs}(x, y, t)$ is non-uniform instead of a scalar $\Sigma_{H,0}$ in (7). Moreover, $\Sigma_{H,QSAPs}$ was assumed to change so as to satisfy the equation

$$\frac{\partial \Sigma_{H,QSAPs}}{\partial t} + \nabla \cdot \left(\Sigma_{H,QSAPs} \mathbf{v}_\perp \right) = 0. \qquad (8)$$

Equation (8) indicates that the QSAPs move with the ionospheric plasma and the total amount of the source of the QSAPs (q_{QSAPs}) is constant, because q_{QSAPs} is proportional to $\Sigma_{H,QSAPs}$.

[35] $j_{z,M}$ on the top of the AAR was associated with the FLRs. The magnetic perturbations, b_x, of the toroidal mode

oscillations due to the FLRs are often approximated by the driven damped harmonic oscillation as shown below:

$$\ddot{b}_x + 2\gamma\dot{b}_x + \omega_R^2 b_x = \omega_R^2 c \cdot \sin(\omega_D t), \qquad (9)$$

where ω_R (y), ω_D, γ, and c are the undamped angular frequency corresponding to the resonant frequency, the driving frequency, the dumping ratio, and a constant associated with the amplitude of the fast mode waves [*Gough and Orr*, 1984; *Menk et al.*, 1994]. It was assumed that ω_R depends on y only and thus b_x is a function of y and uniform in the x direction. The general solution of (9) is known to be

$$b_x = a e^{-\gamma t} \sin\left(\sqrt{\omega_R^2 - \gamma^2} \, t + \epsilon \right) + A \sin(\omega_D t - \delta), \qquad (10)$$

where a and ϵ are constants and A and δ are given by

$$A = \frac{c\omega_R^2}{\sqrt{\left(\omega_R^2 - \omega_D^2\right)^2 + 4\gamma^2\omega_D^2}}, \qquad (11)$$

$$\delta = \tan^{-1}\left(\frac{2\gamma\omega_D}{\omega_R^2 - \omega_D^2} \right). \qquad (12)$$

The first and second terms of the right-hand side of (10) are the transient solution and the steady state solution, respectively. The first term is damped with a damping constant γ. The PMAAs due to the first term were discussed by *Kozlovsky and Kangas* [2002]. In this paper we assumed a monochromatic source and consider only the second term of (10). $j_{z,M}$ was obtained from Ampère's law ($j_{z,M} = -\mu_0^{-1} \, \partial b_x / \partial y$).

[36] For simplicity, we assumed that the FLRs have already been formed at the beginning of the calculation and A and δ do not change temporally. This assumption is not practical, because reflected waves from the ionosphere change with the temporal variation of the conductivities.

[37] The latitudinal distribution of ω_R ($=2\pi/T_R$) was calculated using the approximation of the fundamental toroidal eigenperiod discussed by *Vellante and Förster* [2006, equation (8)], assuming the Tsyganenko 96 magnetic field model [*Tsyganenko*, 1995] and an inverse power law radial density variation along the field lines, $\rho_M = \rho_{M,eq}(r/r_{eq})^{-3}$, where ρ_M and r are the ion mass density and radial distance from the center of the earth. We found that the equatorial ion mass density, $\rho_{M,eq}$, on the field line threading SPA is 0.24 amu/cc, which matches the resonance frequency at SPA (ω_R at $y = 0$) with the observed Pc 5 frequency. The radial profile of $\rho_{M,eq}$ was assumed to be equal to that of the equatorial electron number density, $n_{M,eq}$. The equatorial electron density was derived from *Carpenter and Anderson* [1992, equation (6)], where the second term of the equation was ignored because it causes an increase of the electron density with L at very large L. We multiplied the radial density profile by a constant to fit $\rho_{M,eq}$ at SPA to 0.24 amu/cc. The calculated resonant period, T_R, is presented in Figure 7. ω_D was assumed to be the same as ω_R at $y = 0$.

[38] The magnetic field observed on the ground can be obtained from the ionospheric current. The total ionospheric
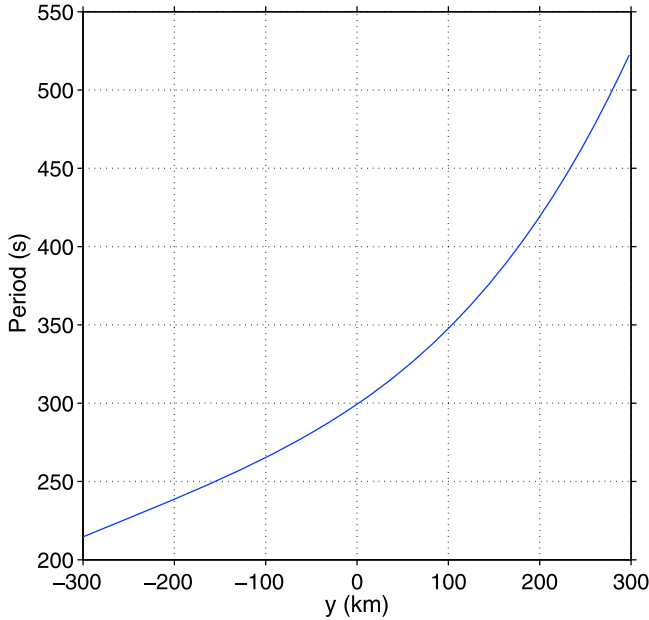
Figure 7. Latitudinal distribution of the FLR frequency assumed for the numerical simulation.

Figure 8. Height-integrated Hall conductivity (Σ_H) calculated from the simulation. The top and right of each panel correspond to the south and west, respectively.

current was first separated into the divergence-free and the curl-free vector fields. Since the ground magnetic field generated from the curl-free ionospheric current is canceled by that from FACs, the ground magnetic field was calculated from the divergence-free current by Biot–Savart's law [e.g., *Raeder et al.*, 2001, equations (22)–(29)]. It was assumed
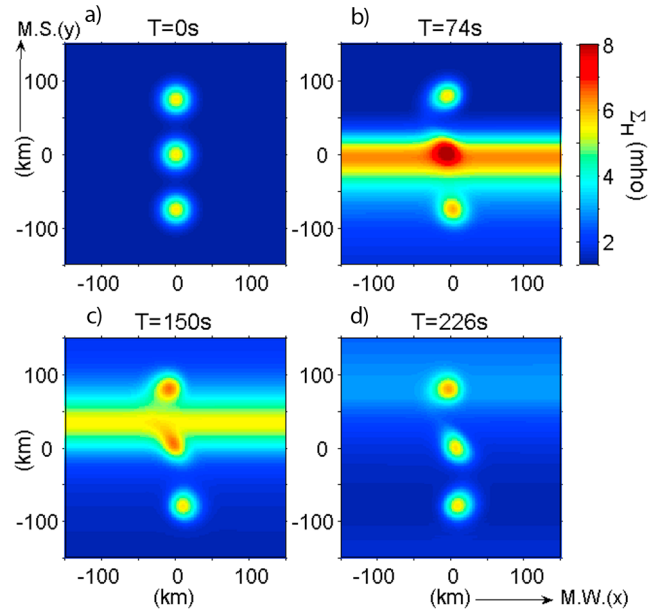
that the ionospheric current flows at 110 km altitude and the solid Earth is a perfect conductor.

[39] The parameters used in the calculation are summarized in Table 1. We adjusted the parameters c, K, and $\Sigma_{H,0}$ so as to match the simulation results with the observed data (V_W, B_N, and I_{5577}).

Table 1. Simulation Parameters

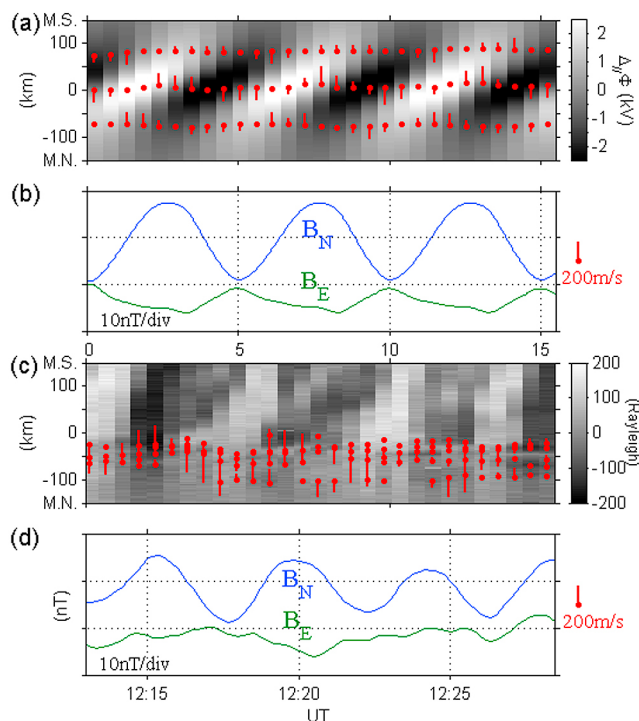| Symbol	Value	Explanation
K	2.0×10^{-10} mho m^{-2}	K is generally assumed to be between 10^{-8} and 10^{-10} mho m^{-2} [*Olsson et al.*, 1996]. It satisfies the equation $K \approx e^2 n_M / \sqrt{2\pi m_e k_B T_M}$.
$F_{P,H}(z)$	-	$F_{P,H}(z)$ are calculated based on *Richmond* [1995]. $F_{P,H}(z)$ need n_{N_2}, n_{O_2}, n_O, n_{O^+}, $n_{O_2^+}$, n_{NO^+}, T_i, T_e, T_n, and B_0, calculated from MSISE90, IRI2000, IGRF models [*Hedin*, 1991; *Bilitza*, 2001; *International Association of Geomagnetism and Aeronomy, Division V, Working Group VMOD: Geomagnetic Field Modeling*, 2005].
$\alpha(z)$	$4.30 \times 10^{-12} \exp(-2.42 \times 10^{-2} z)$ +8.16 $\times 10^6 \exp(-0.524z)$ [m^{3}s^{-1}] (z is in km)	*Gledhill*, [1986]
$\rho(z)$	-	$\rho(z)$ was obtained from MSISE90 model [*Hedin*, 1991].
$\Delta\epsilon_{ion}$	35.5 eV	*Rees* [1989]
$\lambda(z, E)$	-	*Semeter and Kamalabadi* [2005, Table 1]
$R(E)$	$4.30 \times 10^{-6} + 5.36 \times 10^{-5} E^{1.67}$ [kg m^{-2}] (E is in keV)	*Rees* [1989]
n_M	0.24×10^6 m^{-3}	It was assumed that n_M is equal to $n_{M,eq}$ and the ions consist of protons only.
$k_B T_M$	1 keV	Thermal energy of source electrons
$\Sigma_{H,0}$	1.3 mho	Background Hall conductivity
$\Sigma_{H,QSAPs}(t=0s)$	-	Gaussian distribution with a maximum of 4 mho
γ	$0.1\ \omega_R$	Damping ratio
$T_D\ (=2\pi/\omega_D)$	300 s	Period of driving waves
Δt	2 s	Time step
x_{min}–x_{max}	-300–300 km	Spatial range in x (=y_{min}–y_{max})
z_{min}–z_{max}	80–200 km	Altitude range
Δ_x	2 km	Grid spacing in x (=Δ_y)
Δ_z	4 km	Grid spacing in z
E_{min}–E_{max}	0.3–20 keV	Energy range
N_E	30	Number of energy grid. The energy range is divided by N_E logarithmically.

Figure 9. (a) N-S keogram of the field-aligned potential drop with the E-W drift velocity of the auroral patches and (b) magnetic field on the ground obtained from the numerical simulation. (c) N-S keogram of the 557.7-nm intensity with the E-W drift velocity of the QSAPs and (d) magnetic field on the ground observed in the interval 12:13–12:29 UT.

[40] Figure 8 shows the temporal variation of Σ_H calculated from the simulation. As seen in Figure 8a, it was assumed that the QSAPs at $t = 0$ s were located at $(x, y) = (0, -75)$, $(0, 0)$, and $(0, 75)$ in km and the shape of the QSAPs is the Gaussian distribution. The E-W elongated enhanced Σ_H in Figures 8b–8d that propagates poleward corresponds to the PMAAs. The QSAPs oscillate dominantly in the E-W direction as the PMAAs pass over the QSAPs. It can be found that the QSAPs move eastward on the south side of the arc and westward on the north side.

[41] Here, we attempt to reproduce the observed data from the simulation results. The results are presented in Figures 9a and 9b, together with the data observed at 12:13–12:29 UT in Figures 9c and 9d. Figure 9a shows the N-S keogram of the field-aligned potential drop ($\Delta_\parallel\Phi$) with the E-W drift velocity of the assumed patches obtained from the simulation. The positive $\Delta_\parallel\Phi$ indicates an upward FAC and electron precipitation, corresponding to the auroral emission. For a comparison with the observation, these data were sampled every 32 s from the simulation results. The calculated N-S and E-W components of the ground magnetic field are presented in Figure 9b. The simulated data are quite similar to the observed data. It is clear that the three phenomena have a high correlation coefficient and almost the same dominant frequencies. The amplitude of B_N and V_W are about 8 nT and 200 m/s, respectively, which are comparable to the observed values. $\Delta_\parallel\Phi$ is about 3 kV at maximum and is large enough to excite the 557.7-nm emission. The observed

in-phase relation between B_N and V_W is also reproduced well by the simulation.

[42] On the other hand, it is difficult to explain the antiphase relation of the PMAAs with respect to B_N and V_W, because it is expected from the simulation that the PMAAs precede B_N and V_W by 90°. The discrepancy between the observation and simulation may be attributed to the weak and broad auroral arcs. The PMAAs analyzed in this paper were much weaker and latitudinally broader than typical PMAAs [e.g., *Milan et al.*, 1999a, 2001]. The broad arcs are consistent with the relatively small latitudinal phase variation in Figure 4, which is smaller than that reported by *Milan et al.* [1999a, 2001], who showed a 180° phase shift within 1° latitude across the latitude of maximum emission intensity. The broad latitudinal wave structure of the arcs may cause difficulties in determining the phase relation between the auroral luminosity and the ionospheric flow.

[43] The attenuation of the PMAAs after 15:00 UT (item 5 of the observation summary) may also be explained by this model. By rewriting the current continuity equations (1) and (2), the field-aligned potential drop is appropriated by

$$\Delta_\parallel\Phi = \frac{-1}{K}\nabla_\perp \cdot \left(\Sigma_P \mathbf{E}_{\perp,I} + \Sigma_H \hat{\mathbf{e}}_z \times \mathbf{E}_{\perp,I}\right) \approx -\frac{ik_y}{K}\Sigma_P E_{y,I}, \quad (13)$$

where $\mathbf{E}_{\perp,I}$ is the horizontal component of the ionospheric electric field and k_y is the meridional wave number. It is deduced from the westward drift velocity in Figure 4 that $E_{y,I}$ associated with the Pc 5 pulsations after 14:00 UT is smaller by roughly half than that before 14:00 UT. This is also supported by the attenuation in the amplitude of the Pc5 pulsations after 14:00 UT (Figure 2b). Moreover, k_y should be smaller after 15:00 UT than before 14:00 UT, because the dominant period of the Pc 5 pulsations is much longer after 15:00 UT ($\sim$620 s) than before 14:00 UT ($\sim$330 s) and thus the phase variation along the meridian is smaller. Therefore, it is reasonable to assume that the field-aligned potential drop after 15:00 UT is too small to generate the PMAAs.

6. Conclusions

[44] The PMAAs, the Pc 5 pulsations, and the oscillations in the drift of the QSAPs observed at SPA (74.3 CGLAT) in the interval 08:00–11:00 MLT showed good correlations, similar dominant periods, and a systematic phase difference between each other. They occurred during the northward IMF condition and in the closed field lines, because the QSAPs at 557.7 nm were located at lower latitudes than the LLBL or the cleft region and similar Pc 5 pulsations were observed at a geomagnetic conjugate station of SPA, IQA in the northern hemisphere. Hence, FLRs are the most probable generation mechanism of these three phenomena. The numerical simulation using 2-D models that consist of the AAR and the ionosphere clarified that the FLR model can reasonably explain most of the observed data, i.e., the amplitude of the Pc 5 pulsations in the N-S component (B_N), the E-W drift velocity of the QSAPs (V_W), the 557.7-nm emission corresponding to the field-aligned potential drop greater than 1 kV, and the in-phase relation between B_N and V_W. Therefore, we conclude that the PMAAs, the Pc 5 pulsations, and the oscillations in the drift of the QSAPs shown in this paper are various aspects of the FLRs. On the

other hand, the phase relation of the PMAAs with the other two phenomena remains a puzzle and will be explored in future research.

References

Bilitza, D. (2001), International Reference Ionosphere 2000, *Radio Sci.*, *36*(2), 261–275.

Carpenter, D. L., and R. R. Anderson (1992), An ISEE/whistler model of equatorial electron density in the magnetosphere, *J. Geophys. Res.*, *97*(A2), 1097–1108, doi:10.1029/91JA01548.

Chen, L., and A. Hasegawa (1974), A theory of long-period magnetic pulsations: 1. Steady state excitation of field line resonance, *J. Geophys. Res.*, *79*, 1024–1032.

Drury, E. E., S. B. Mende, H. U. Frey, and J. H. Doolittle (2003), Southern Hemisphere poleward moving auroral forms, *J. Geophys. Res.*, *108*(A3), 1114, doi:10.1029/2001JA007536.

Ebihara, Y., Y.-M. Tanaka, S. Takasaki, A. T. Weatherwax, and M. Taguchi (2007), Quasi-stationary auroral patches observed at the South Pole Station, *J. Geophys. Res.*, *112*, A01201, doi:10.1029/2006JA012087.

Farrugia, C. J., P. E. Sandholt, N. C. Maynard, W. J. Burke, J. D. Scudder, D. M. Ober, J. Moen, and C. T. Russell (2000), Pulsating midmorning auroral arcs, filamentation of a mixing region in a flank boundary layer, and ULF waves observed during a Polar-Svalbard conjunction, *J. Geophys. Res.*, *105*(A12), 27,531–27,553.

Fasel, G. J. (1995), Dayside poleward moving auroral forms: A statistical study, *J. Geophys. Res.*, *100*(A7), 11,891–11,905, doi:10.1029/95JA00854.

Fridman, M., and J. Lemaire (1980), Relationship between auroral electron fluxes and field aligned electric potential difference, *J. Geophys. Res.*, *85*, 664–670.

Gledhill, J. A. (1986), The effective recombination coefficient of electrons in the ionosphere between 50 and 150 km, *Radio Sci.*, *21*(3), 399–408.

Gough, H., and D. Orr (1984), The effect of damping on geomagnetic pulsation amplitude and phase at ground observatories, *Planet. Space Sci.*, *32*(5), 619–628.

Hedin, A. E. (1991), Extension of the MSIS thermosphere model into the middle and lower atmosphere, *J. Geophys. Res.*, *96*, 1159–1172.

International Association of Geomagnetism and Aeronomy, Division V, Working Group VMOD: Geomagnetic Field Modeling (2005), The 10th-Generation International Geomagnetic Reference Field, *Geophys. J. Int.*, *161*, 561–565.

Janhunen, P., and A. Huuskonen (1993), A numerical ionosphere-magnetosphere coupling model with variable conductivities, *J. Geophys. Res.*, *98*(A6), 9519–9530, doi:10.1029/92JA02973.

Karlson, K. A., M. Oieroset, J. Moen, and P. E. Sandholt (1996), A statistical study of flux transfer event signatures in the dayside aurora: The IMF By-related prenoon–postnoon asymmetry, *J. Geophys. Res.*, *101*, 59–68.

Knight, S. (1973), Parallel electric fields, *Planet. Space Sci.*, *21*, 741–750.

Kozlovsky, A., and J. Kangas (2002), Motion and origin of noon high-latitude poleward moving auroral arcs on closed magnetic field lines, *J. Geophys. Res.*, *107*(A2), 1017, doi:10.1029/2001JA900145.

Lyons, L. R., D. S. Evans, and R. Lundin (1979), An observed relation between magnetic field aligned electric fields and downward electron energy fluxes in the vicinity of auroral forms, *J. Geophys. Res.*, *84*, 457–461.

Menk, F. W., B. J. Fraser, C. L. Waters, C. W. S. Ziesolleck, Q. Feng, S. H. Lee, and P. W. McNabb (1994), Ground measurements of low latitude magnetospheric field line resonances, in *Solar Wind Sources of Magnetospheric Ultra-Low-Frequency Waves*, *Geophys. Monogr. Ser.*, vol. 81, edited by M. J. Engebreston, K. Takahashi, and M. Scholer, pp. 299–310, AGU, Washington, D. C., doi:10.1029/GM081p0299.

Milan, S. E., T. K. Yeoman, M. Lester, J. Moen, and P. E. Sandholt (1999a), Post-noon two-minute period pulsating aurora and their relationship to the dayside convection pattern, *Ann. Geophys.*, *17*, 877–891.

Milan, S. E., M. Lester, S. W. H. Cowley, J. Moen, P. E. Sandholt, and C. J. Owen (1999b), Meridian-scanning photometer, coherent HF radar, and magnetometer observations of the cusp: A case study, *Ann. Geophys.*, *17*, 159–172.

Milan, S., N. Sato, M. Ejiri, and J. Moen (2001), Auroral forms and the field-aligned current structure associated with field line resonances, *J. Geophys. Res.*, *106*(A11), 25,825–25,833, doi:10.1029/2001JA900077.

Oguti, T., R. Nakamura, and T. Yamamoto (1987), Oscillations in drifts of auroral patches, *J. Geomagn. Geoelectr.*, *39*, 609–624.

Olsson, A., A. I. Eriksson, and P. Janhunen (1996), On the current–voltage relationship in auroral breakups and westwards-travelling surges, *Ann. Geophys.*, *14*, 1265–1273.

Poulter, E. M. (1982), Pc 5 micropulsation resonance regions observed with the STARE radar, *J. Geophys. Res.*, *87*, 8167–8173, doi:10.1029/JA087iA10p08167.

Raeder, J., R. L. McPherron, L. A. Frank, S. Kokubun, G. Lu, T. Mukai, W. R. Paterson, J. B. Sigwarth, H. J. Singer, and J. A. Slavin (2001), Global simulation of the Geospace Environment Modeling substorm challenge event, *J. Geophys. Res.*, *106*(A1), 381–395.

Rees, M. H. (1989), *Physics and Chemistry of the Upper Atmosphere*, edited by J. T. Houghton, M. J. Rycroft, and A. J. Dessler, Cambridge Univ. Press, New York.

Richmond, A. D. (1995), Ionospheric electrodynamics, in *Handbook of Atmospheric Electrodynamics*, vol. 2, 249–290, CRC Press, Boca Raton, Fla.

Samson, J. C., T. J. Hughes, F. Creutzberg, D. D. Wallis, R. A. Greenwald, and J. M. Ruohoniemi (1991), Observations of a detached, discrete arc in association with field line resonances, *J. Geophys. Res.*, *96*(A9), 15,683–15,695, doi:10.1029/91JA00796.

Samson, J. C., L. L. Cogger, and Q. Pao (1996), Observations of field line resonances, auroral arcs, and auroral vortex structures, *J. Geophys. Res.*, *101*(A8), 17,373–17,383, doi:10.1029/96JA01086.

Sandholt, P. E., M. Lockwood, T. Oguti, S. W. H. Cowley, K. S. C. Freeman, B. Lybekk, A. Egeland, and D. M. Willis (1990), Midday auroral breakup events and related energy and momentum transfer from the magnetosheath, *J. Geophys. Res.*, *95*, 1039–1060.

Sandholt, P. E., J. Moen, A. Rudland, D. Opsvik, W. F. Denig, and T. Hansen (1993), Auroral event sequences at the dayside polar cap boundary for positive and negative IMF B$_Y$, *J. Geophys. Res.*, *98*, 7737–7755.

Semeter, J., and F. Kamalabadi (2005), Determination of primary electron spectra from incoherent scatter radar measurements of the auroral E region, *Radio Sci.*, *40*, RS2006, doi:10.1029/2004RS003042.

Southwood, D. J. (1974), Some features of field line resonances in the magnetosphere, *Planet. Space Sci.*, *22*, 483–491.

Tamao, T. (1964), The structure of three-dimensional hydromagnetic waves in a uniform cold plasma, *J. Geomagn. Geoelectr.*, *18*, 89–114.

Tanaka, Y.-M., T. Aso, B. Gustavsson, K. Tanabe, Y. Ogawa, A. Kadokura, H. Miyaoka, T. Sergienko, U. Brändström, and I. Sandahl (2011), Feasibility study on generalized-aurora computed tomography, *Ann. Geophys.*, *29*, 551–562, doi:10.5194/angeo-29-551-2011.

Tsyganenko, N. A. (1995), Modeling the Earth's magnetospheric magnetic field confined within a realistic magnetopause, *J. Geophys. Res.*, *100*, 5599–5612.

Vellante, M., and M. Förster (2006), Inference of the magnetospheric plasma mass density from field line resonances: A test using a plasmasphere model, *J. Geophys. Res.*, *111*, A11204, doi:10.1029/2005JA011588.

Walker, A. D. M., and R. A. Greenwald (1981), Statistics of occurrence of hydromagnetic oscillations in the Pc5 range observed by the STARE auroral radar, *Planet. Space Sci.*, *29*, 293–305.

Walker, A. D. M., R. A. Greenwald, W. F. Stuart, and C. A. Green (1979), STARE auroral radar observations of Pc5 geomagnetic pulsations, *J. Geophys. Res.*, *84*, 3373–3388.

Yamamoto, T., et al. (1988), Auroral activities and long-period geomagnetic pulsations: 1 Pc5 pulsations and concurrent auroras in the dawn sector, *J. Geomagn. Geoelectr.*, *40*, 553–569.